The Plant Cell, Vol. 32: 3812–3824, December 2020, www.plantcell.org © 2020 ASPB.

Transcriptional Regulation of *PLETHORA1* in the Root Meristem Through an Importin and Its Two Antagonistic Cargos

Feng Xiong,[a] Bi-Ke Zhang,[a] Hai-Hong Liu,[a] Guo Wei,[a] Ju-Hua Wu,[a] Ya-Nan Wu,[a] Yan Zhang,[a] and Sha Li[a,b,1]

[a] State Key Laboratory of Crop Biology, College of Life Sciences, Shandong Agricultural University, Tai'an 271018, China
[b] Department of Plant Biology and Ecology, College of Life Sciences, Nankai University, Tianjin 300071, China

Plant roots are sustained through meristem activity at the root tip. Two transcriptional pathways, one mediated by PLETHORAs (PLTs) and the other by SHORTROOT and SCARECROW, play major roles in root meristem development. The role of PLTs during root meristem development requires a concentration gradient, which is not only contributed by posttranslational regulation such as growth dilution and intercellular movement but also likely by a largely unknown fine-tuned transcriptional regulatory mechanism. We report here that Arabidopsis (*Arabidopsis thaliana*) JANUS positively regulates *PLT1* expression in the root meristem by recruiting RNA polymerase II (Pol II) to *PLT1* and by interacting with PLT1. JANUS-dependent recruitment of Pol II is inhibited through the competitive binding of JANUS by GRF-INTERACTING FACTOR1 (GIF1)/ANGUSTIFOLIA3, a transcriptional cofactor that negatively regulates *PLT1* expression. Finally, GIF1 and JANUS, the antagonistic regulators of *PLT1*, both depend on Arabidopsis IMPORTIN β4 for their nuclear accumulation. The combination of an importin and its two antagonistic cargos in *PLT1* transcription may have logistic benefits in fine-tuning the transcription of *PLT1* in root meristem.

INTRODUCTION

The activity of the meristem at the root tip sustains plant root growth. The root meristem is organized into well-defined domains, like the stem cell niche and transit-amplifying cells produced by root stem cells (Dolan et al., 1993; Watt and Hogan, 2000; Weigel and Jürgens, 2002; Laux, 2003; Aida et al., 2004). The root stem cell niche consists of the quiescent center (QC) and surrounding stem cells. Stem cells are pluripotent cells whose progeny normally generate defined yet flexible cell types, depending on their position (Xu et al., 2006; Scheres, 2007; Sena et al., 2009), while QC cells are mitotically inactive but are critical for maintaining and replenishing stem cells (Dolan et al., 1993; van den Berg et al., 1995; Cruz-Ramírez et al., 2013).

Two major transcriptional routes specify the QC cell fate and the adjacent stem cells: PLETHORA family members (PLTs) and SHORTROOT/SCARECROW (SCR; Wysocka-Diller et al., 2000; Sabatini et al., 2003; Aida et al., 2004; Heidstra et al., 2004; Galinha et al., 2007; Scheres, 2007; Heidstra and Sabatini, 2014). Mutations in either pathway cause the collapse of the QC and the disorganization of stem cells, thereby compromising root growth and meristem development (Petricka et al., 2012; Heyman et al., 2014; Shimotohno et al., 2018). The establishment and maintenance of a PLT concentration gradient is critical for root development, such that higher PLT levels promote stem cell maintenance while lower PLT levels promote the mitotic activity of stem cell daughters (Galinha et al., 2007; Mahönen et al., 2014). A further reduction in PLT levels promotes cell differentiation (Mahönen et al., 2014). The PLT gradient controls cell fate by the spatial induction of genes required for cell proliferation and the repression of genes involved in cell differentiation (Santuari et al., 2016). Moreover, PLT targets include major patterning genes and components of an autoregulatory feedback loop, thus reenforcing their key roles in organ development (Santuari et al., 2016). Growth dilution and intercellular movement both contribute to the establishment of the PLT gradient (Mahönen et al., 2014). However, it is not fully understood how transcriptional regulation influences this protein gradient.

A recent study demonstrated that the transcriptional coactivator GRF-INTERACTING FACTOR1 (GIF1)/ANGUSTIFOLIA3 negatively regulates *PLT1* expression, likely by interacting with transcription factors such as GROWTH REGULATORY FACTORS (GRFs) in the root meristem (Rodriguez et al., 2015; Ercoli et al., 2018). We recently demonstrated that the Arabidopsis (*Arabidopsis thaliana*) importin, IMPORTIN β4 (IMB4), mediates the nuclear accumulation of GIF1 (Liu et al., 2019). However, in contrast to the longer roots seen in *gif1* mutants (Ercoli et al., 2018), null mutants for *IMB4* showed reduced root growth (Liu et al., 2019), suggesting a complexity in their interaction. Here, we report that IMB4 mediates the nuclear accumulation of another transcriptional regulator of *PLT1*, JANUS, in addition to that of GIF1. JANUS positively regulates the expression of *PLT1* in the root meristem by recruiting RNA polymerase II (Pol II). Interestingly, GIF1 inhibits the binding of Pol II with JANUS through competitive binding with the RNA recognition motif II (RRM2) domain of JANUS. Furthermore, JANUS directly interacts with PLT1 via its C terminus and is required for the autotranscriptional regulation of PLT1. Thus, GIF1 and JANUS, whose nuclear accumulation is controlled by IMB4, antagonistically mediate root meristematic activity. Such a tripartite module may fine-tune the expression of *PLT1* to control root meristem homeostasis.

[1] Address correspondence to shali@sdau.edu.cn.
The author responsible for distribution of materials integral to the findings presented in this article in accordance with the policy described in the Instructions for Authors (www.plantcell.org) is: Sha Li (shali@sdau.edu.cn).
www.plantcell.org/cgi/doi/10.1105/tpc.20.00108

IN A NUTSHELL

Background: Spatially coordinated cell division and differentiation during the development of the root meristem (RAM) are critical steps for sustained root growth in plants. Recent studies demonstrated that the transcription factor PLETHORA1 (PLT1) forms a concentration gradient to control RAM development. However, how the transcriptional regulation of *PLT1* contributes to its protein gradient remains unknown. Two Arabidopsis proteins we have been working on, JANUS and IMPORTIN β4 (IMB4), play positive yet unclear roles in root growth. JANUS is a putative spliceosome subunit with transcriptional activity through its binding to RNA polymerase II (Pol II), while IMB4 is involved in protein trafficking between the nucleus and the cytoplasm or in maintaining protein stability.

Question: We aimed to identify the transcriptional pathways that act upstream of *PLT1* and understand the complexity of the underlying regulatory networks controlling RAM development.

Findings: We discovered that Arabidopsis PLT1 activates its own transcription and that this auto-transcriptional regulation relies on JANUS. JANUS interacts with PLT1 and Pol II through different domains to facilitate *PLT1* transcription. The JANUS-dependent *PLT1* auto-transcriptional activation potentially amplifies the PLT1 gradient established by mitotic dilution and intercellular movement: it is thus critical for the maintenance of sufficiently high levels of PLT1 during RAM development. By contrast, a transcriptional co-factor, GRF-INTERACTING FACTOR1/ANGUSTIFOLIA3 (GIF1/AN3), interacts with JANUS to deplete it from the JANUS-Pol II transcriptional complex, therefore negatively regulating JANUS-dependent *PLT1* transcription. As an additional layer of complexity, GIF1/AN3 and JANUS both rely on IMB4 for their nuclear accumulation.

Next steps: That two interacting but antagonistic regulators of *PLT1* are regulated by the same importin raises the following question: how is selectivity of interaction between IMB4, JANUS, and GIF1/AN3 spatially controlled in the context of root development? Plant genomes encode few importins, even though the demand for nucleo-cytoplasmic shuttling is tremendous. Whether one importin is truly responsible for various cargos in the same signaling pathway for logistical benefits is certainly worthy of future investigation.

RESULTS AND DISCUSSION

Functional Loss of *IMB4* Compromises Root Meristem Activity

The nuclear accumulation of GIF1 in ovules depends on IMB4 (Liu et al., 2019). Indeed, *imb4-1*, a null mutation of *IMB4*, shows defective ovule development comparable to that of *gif1* (Liu et al., 2019). We determined that root apical meristem (RAM) cells in *imb4-1* exhibit a significant reduction of nuclear GIF1 accumulation compared with the wild type (Supplemental Figure 1) even though *IMB4* is highly expressed in roots (Figure 1A), based on confocal laser scanning microscopy (CLSM) of the *IMB4g*-GFP construct in transgenic plants (Liu et al., 2019). Thus, we expected a longer RAM in the *imb4-1* mutant, as seen in *gif1* or higher-order mutants of *GIF* family members (Ercoli et al., 2018). However, *imb4-1* instead showed a significantly reduced root meristem (Figures 1B and 1D), which resulted from a reduced activity in cell division (Figures 1C and 1E). The genes *PLT1*, *PLT2*, and *SCR*, which are critical for root meristem development (Wysocka-Diller et al., 2000; Sabatini et al., 2003; Aida et al., 2004; Heidstra et al., 2004; Galinha et al., 2007; Scheres, 2007; Petricka et al., 2012; Heidstra and Sabatini, 2014; Heyman et al., 2014; Shimotohno et al., 2018), were all transcriptionally downregulated in the *imb4-1* mutant relative to the wild type, based on the analysis of their respective reporter lines in which the expression of *Cyan Fluorescent Protein* (*CFP*) or *Yellow Fluorescent Protein* (*YFP*) is driven by their native promoters (Figures 1F to 1K): *PLT1pro*:CFP (Chen et al., 2011), *PLT2pro*:CFP (Chen et al., 2011), or *SCRpro*:H2B-YFP (Heidstra et al., 2004). RT-qPCR independently validated these results (Figures 1L to 1N), thus suggesting that IMB4 plays a positive role in root meristem development.

IMB4 Mediates the Nuclear Accumulation of JANUS

The fact that *imb4-1* differed from *gif1*, a mutant in one of its cargos (Liu et al., 2019) during root meristem development, suggested that other IMB4 cargos might play positive roles in this process. By screening the Arabidopsis Protein Interactome Database (Li et al., 2011), we focused on JANUS out of a few potential IMB4 interactors. JANUS is a putative component of the spliceosome (Xiong et al., 2019a; Xiong and Li, 2020) that was recently demonstrated to recruit Pol II for the transcription of *WUSCHEL-RELATED HOMEOBOX2* (*WOX2*) and *PIN-FORMED7* (*PIN7*) during embryogenesis (Xiong et al., 2019a). Indeed, JANUS interacted with IMB4 by yeast two-hybrid (Y2H; Figure 2A), by bimolecular fluorescence complementation (BiFC; Figure 2B), and by in vitro pull-down (Figure 2C) assays.

To determine how IMB4 might regulate JANUS, we analyzed GFP distribution in the root meristem of the wild type or the *imb4-1* mutant expressing the *JANUSg*-GFP construct by CLSM. *JANUSg*-GFP rescues the embryo lethality normally seen in *janus* mutants (Xiong et al., 2019a), indicating that the JANUS-GFP fusion protein is functional. We detected strong GFP signal in the nuclei of wild-type cells but not in *imb4-1* (Figures 2D and 2E), although *JANUSg*-GFP was expressed at a comparable level in the wild type and *imb4-1* (Supplemental Figure 2B), suggesting the IMB4-dependent nuclear accumulation of JANUS. Indeed, inhibiting 26S proteasome-mediated degradation with the proteasome inhibitor MG132 substantially increased the nuclear intensity of the JANUS-GFP fusion protein in both the wild type and *imb4-1* (Figures 2D and 2E), indicating that IMB4 protects JANUS against 26S proteasome-mediated degradation. In addition, GFP signal appeared in the cytoplasm in both the wild type and *imb4-1* upon MG132 treatment (Figures 2D and 2E),

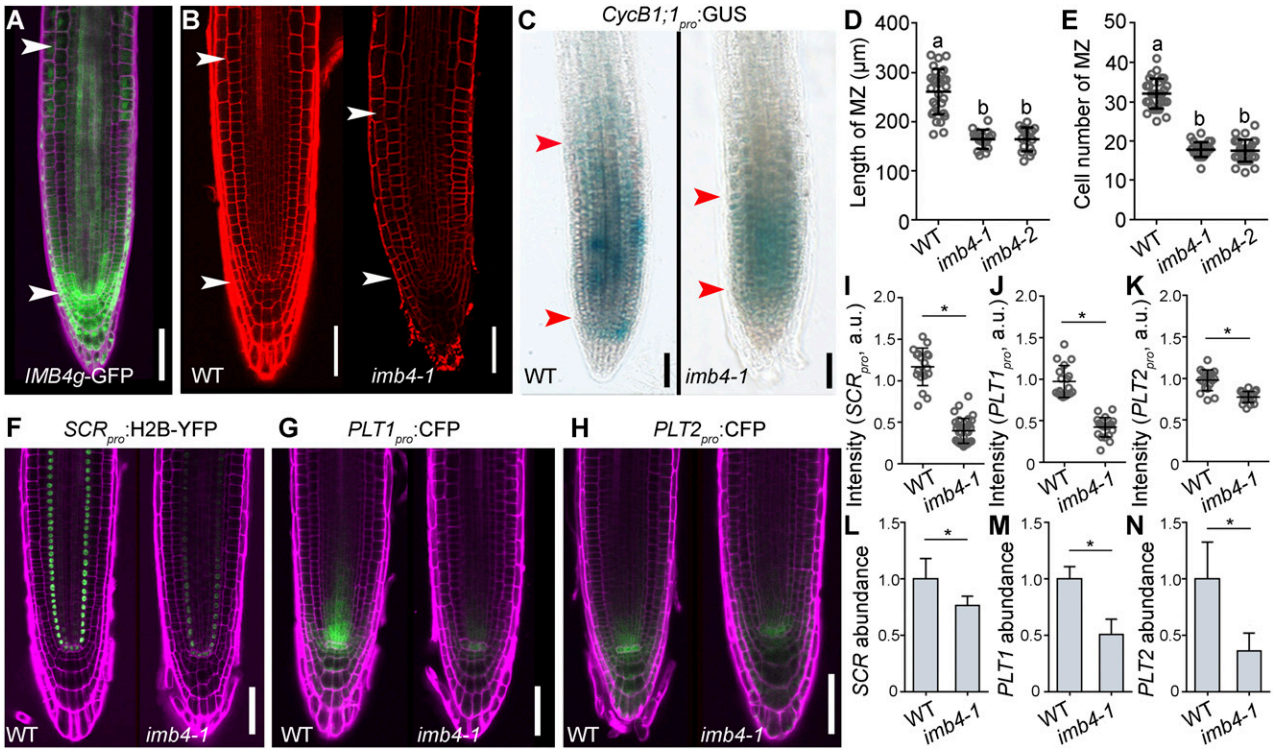

Figure 1. Functional Loss of *IMB4* Compromises Root Meristem Activity.

(A) Representative CLSM image of an *IMB4g*-GFP seedling root. The root was stained with propidium iodide (PI; magenta).
(B) Representative CLSM images of PI-stained wild-type and *imb4-1* roots.
(C) *CycB1;1pro*:GUS activity in wild-type and *imb4-1* roots.
The region of the RAM is indicated by two arrowheads in **(A)** to **(C)**.
(D) and **(E)** Length **(D)** and cell number **(E)** of the root meristem zone (MZ). Values are means ± SD ($n > 16$). Different letters indicate significantly different groups (one-way ANOVA, Tukey's multiple comparisons test, $P < 0.05$).
(F) to **(K)** Representative CSLM images (**[F]** to **[H]**) and fluorescence intensities (**[I]** to **[K]**) of *SCRpro*:H2B-YFP (**[F]** and **[I]**), *PLT1pro*:CFP (**[G]** and **[J]**), and *PLT2pro*:CFP (**[H]** and **[K]**) in wild-type and *imb4-1* roots. a.u. indicates arbitrary units. Roots were stained with PI (magenta). Values are means ± SD ($n > 16$; **[J]** and **[K]**) or means ± SE ($n = 10$; **[I]**). Fluorescence of the nuclei from 10 roots was measured for **(I)**; fluorescence of the stem cell niche from over 16 roots was measured for **(J)** and **(K)**.
(L) to **(N)** Relative transcript abundance for *SCR* **(L)**, *PLT1* **(M)**, and *PLT2* **(N)** 5 d after germination (DAG) in wild-type and *imb4-1* seedlings, as determined by RT-qPCR.
Asterisks in **(I)** to **(N)** indicate significant differences (*t* test, $P < 0.05$). Bars in **(A)** to **(C)** and **(F)** to **(H)** = 50 μm.

suggesting that JANUS undergoes rapid turnover in the cytoplasm. By employing cell fractionation and immunoblot analyses, we confirmed that IMB4 positively regulates the nuclear accumulation of JANUS by preventing 26S proteasome-mediated degradation (Figure 2F). Ivermectin, an inhibitor of nuclear import, significantly inhibited the nuclear accumulation of JANUS-GFP (Supplemental Figure 3), further supporting a dynamic import of JANUS to the nucleus in RAM.

Because JANUS is essential for embryogenesis (Xiong et al., 2019a), it was surprising that the *imb4* mutant would be viable (Liu et al., 2019). A close examination of the expression pattern associated with the *IMB4g*-GFP construct (Liu et al., 2019) showed that *IMB4* is expressed late during embryogenesis—that is, in embryos at the cotyledon stage (Supplemental Figure 2A). In addition, by examining JANUS-GFP distribution in developing embryos, we determined that the nuclear accumulation of JANUS-GFP was comparable between the wild type and the *imb4-1* mutant expressing the *JANUSg*-GFP construct during early embryogenesis. However, GFP signal from the *JANUSg*-GFP transgene was significantly reduced in *imb4-1* embryos at the cotyledon stage compared with wild-type embryos (Supplemental Figures 2C and 2D). These results suggest that nuclear accumulation of JANUS during early embryogenesis is regulated by factors other than IMB4.

JANUS Positively Regulates Root Meristem Activity

To examine the potential role of JANUS in root meristem development, we examined transgenic roots expressing *35Spro*:*JANUS*-RNAi to downregulate *JANUS* transcripts by RNAi interference (RNAi; Xiong et al., 2019a), since *JANUS* loss of function results in embryo lethality (Xiong et al., 2019a). Downregulating *JANUS* indeed caused a severe reduction in root meristem development (Figure 3A). *35Spro*:*JANUS*-RNAi plants

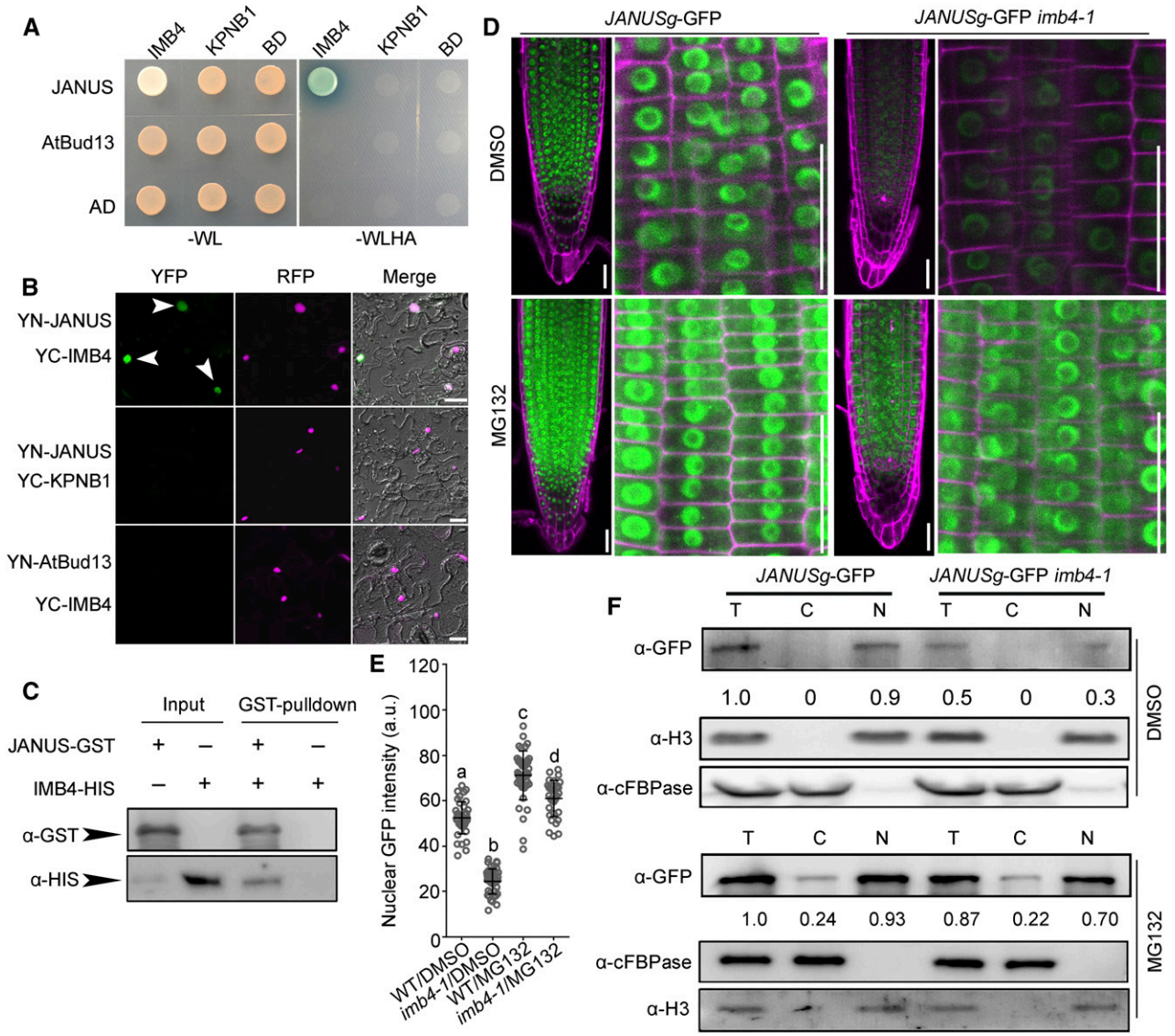

Figure 2. IMB4 Mediates the Nuclear Accumulation of JANUS.

(A) and **(B)** Y2H **(A)** and BiFC **(B)** assays demonstrating the specific interaction between JANUS and IMB4. KPNB1, another Arabidopsis importin β (Luo et al., 2013), was used as a negative control for IMB4, while AtBud13, another component of the spliceosome (Xiong et al., 2019b), was used as a negative control for JANUS. Yeast colonies bearing both the BD and AD vectors were selected on synthetic minimal medium lacking Trp and Leu (–WL); positive interaction was assessed on synthetic minimal medium lacking Trp, Leu, His, and Ade (–WLHA). Bars in **(B)** = 50 μm.

(C) In vitro pull-down assay. Results are representative of three biological replicates.

(D) and **(E)** Representative CLSM images **(D)** and GFP intensities **(E)** of RAM from *JANUSg*-GFP in the wild type and *JANUSg*-GFP in *imb4-1* upon DMSO or MG132 treatment. a.u. indicates arbitrary units. Roots were stained with PI (magenta). Images were taken from seedling roots at 5 DAG treated with DMSO or 100 μM MG132 for 2 h. Values are means ± SE ($n = 20$). Fluorescence of the nuclei in the root meristem zone was measured. Different letters indicate significantly different groups (one-way ANOVA, Tukey's multiple comparisons test, $P < 0.05$). Bars in **(D)** = 50 μm.

(F) Cell fractionation and immunoblot analysis. Anti-GFP antibody was used in immunoblots to detect JANUS-GFP. Numbers at the bottom are the values of JANUS-GFP in the nuclear fraction (N) or cytoplasmic fraction (C) relative to that of the total protein fraction (T), which was set to 1. Anti-histone H3 and anti-cFBPase were used to indicate nuclear and cytoplasmic fractions, respectively.

showed a significantly shorter root meristem (Figure 3C), which was due to reduced cell division (Figures 3B and 3D). By analyzing fluorescence intensity of *SCRpro*:H2B-YFP (Figure 3E), *PLT1pro*:CFP (Figure 3F), or *PLT2pro*:CFP (Figure 3G) in *JANUS*-RNAi lines, we determined that the transcriptional activity at *PLT1* (Figure 3I) and *PLT2* (Figure 3J), but not *SCR* (Figure 3H), was significantly downregulated by *JANUS*-RNAi, which we confirmed by RT-qPCR in wild-type and *JANUS*-RNAi seedlings (Figures 3K to 3M).

Because all three genes are expressed during embryogenesis (Wysocka-Diller et al., 2000; Aida et al., 2004; Xiong et al., 2019a)

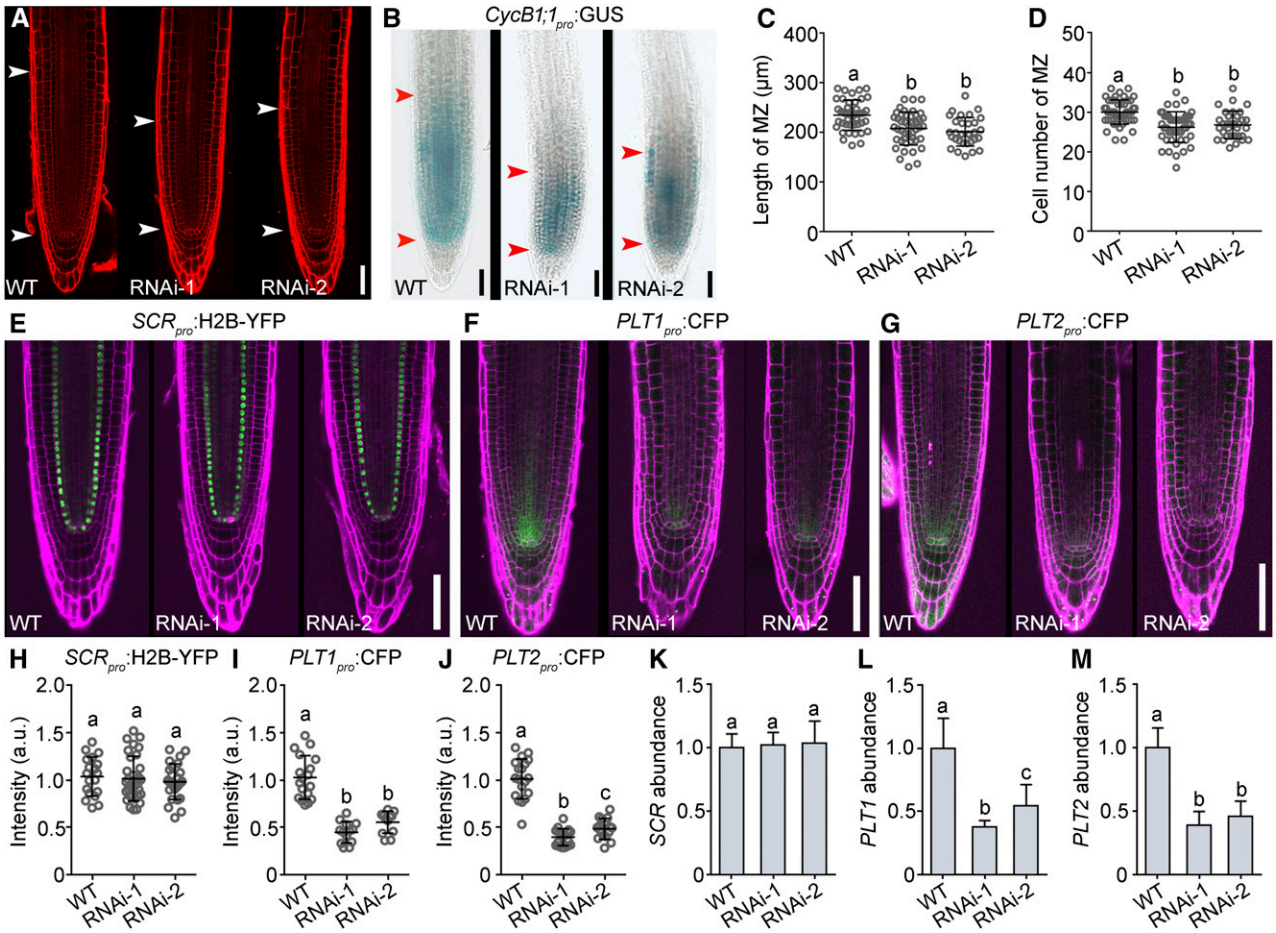

Figure 3. JANUS Positively Regulates Root Meristem Activity.

(A) Representative CLSM image of PI-stained roots from the wild type and two *35Spro*:*JANUS*-RNAi lines (RNAi-1 and RNAi-2).
(B) *CycB1;1pro*:GUS activity in roots from the wild type and two *35Spro*:*JANUS*-RNAi lines.
The region of the RAM is indicated by two arrowheads in **(A)** and **(B)**.
(C) and **(D)** Length **(C)** and cell number **(D)** of the root meristem zone (MZ). Values are means ± SD ($n > 33$).
(E) to **(J)** Representative CSLM images (**[E]** to **[G]**) and fluorescence intensities (**[H]** to **[J]**) of *SCRpro*:H2B-YFP (**[E]** and **[H]**), *PLT1pro*:CFP (**[F]** and **[I]**), and *PLT2pro*:CFP (**[G]** and **[J]**) in the wild type and two *35Spro*:*JANUS*-RNAi lines. a.u. indicates arbitrary units. Roots were stained with PI (magenta). Values are means ± SD ($n > 12$) for **(I)** and **(J)** and means ± SE ($n = 27$) for **(H)**. Fluorescence of the stem cell niche from more than 12 roots was measured for **(I)** and **(J)**; fluorescence of nuclei from 27 roots was measured for **(H)**.
(K) to **(M)** Relative transcript abundance of *SCR* **(K)**, *PLT1* **(L)**, and *PLT2* **(M)** at 5 DAG in the wild type and two lines of *35Spro*:*JANUS*-RNAi by RT-qPCR. Values are means ± SE ($n = 3$).
Different letters in **(C)**, **(D)**, and **(H)** to **(M)** indicate significantly different groups (one-way ANOVA, Tukey's multiple comparisons test, $P < 0.05$). Bars in **(A)**, **(B)**, and **(E)** to **(G)** = 50 μm.

and since JANUS is essential for embryogenesis (Xiong et al., 2019a), we examined developing *janus* embryos expressing the reporters *SCRpro*:H2B-YFP (Supplemental Figure 4A), *PLT1pro*:CFP (Supplemental Figure 4B), or *PLT2pro*:CFP (Supplemental Figure 4C) by CLSM. We obtained results in embryos that were very similar to those seen in the root meristem—that is, the transcriptional activity of *PLT1* and *PLT2* but not *SCR* was substantially downregulated in *janus* embryos (Supplemental Figure 4). These results suggested that JANUS positively regulates root meristem development, possibly by transcriptional regulation of *PLTs*. In addition, JANUS accounts for a specific subset of downstream events mediated by IMB4 during RAM development, since the transcriptional activity of *SCR* was compromised in *imb4-1* (Figure 1) but not in *JANUS*-RNAi lines (Figure 3).

JANUS Mediates Pol II-Dependent *PLT1* Transcription

JANUS was previously demonstrated to recruit Pol II for the transcription of specific genes (Xiong et al., 2019a; Xiong and Li, 2020), despite its lack of obvious DNA binding domains (Xiong et al., 2019a; Xiong and Li, 2020). To test whether the function of JANUS in root meristem was through Pol II, we performed the

following experiments. First, we examined whether the non-catalytic subunit of RNA-dependent RNA polymerase II, IV, and V NRPB10, a JANUS-interacting Pol II component (Xiong et al., 2019a), participated in root meristem development. *NRPB10* is highly expressed in the root meristem (Supplemental Figure 5A), and its loss of function resulted in a significant reduction in root meristem length (Supplemental Figures 5B, 5C, and 5E) and in meristem cell number (Supplemental Figure 5F), suggesting that NRPB10 is a key component of root meristem development. Second, the transcriptional activity at *PLT1* was significantly reduced in the *nrpb10* mutant, based on CFP intensity at the stem cell niche of the *PLT1pro*:CFP reporter expressed in the *nrpb10* background and on RT-PCR (Supplemental Figures 5D, 5G, and 5H). These results suggest that Pol II positively regulates root meristem development by mediating the transcription of key regulatory genes.

Because JANUS specifically recruits Pol II for the transcription of *WOX2* and *PIN7* during embryogenesis (Xiong et al., 2019a), we suspected that the role of Pol II in the transcription of *PLT1* might also depend on JANUS. To test this hypothesis, we examined Pol II occupancy at the *PLT1* promoter by chromatin immunoprecipitation (ChIP) assays (Figure 4A). Indeed, Pol II occupancy was significantly reduced at the promoter regions of *PLT1* by the downregulation of *JANUS* in *JANUS*-RNAi lines or in the *imb4-1* mutant (Figure 4B), indicating that JANUS mediates *PLT1* transcription during root meristem development by recruiting Pol II to the *PLT1* promoter. To provide further evidence that reduced *PLT1* levels resulted from reduced RAM size in *JANUS*-RNAi lines, we introduced *UBQ10pro*:GFP-PLT1 into the *JANUS*-RNAi background. As expected, the ectopic expression of *PLT1* partially rescued the reduced RAM length of *JANUS*-RNAi lines (Figures 4C, 4E, and 4F), consistent with a significant increase in *PLT1* abundance seen by RT-qPCR (Figure 4D). These results suggest that a reduction in *PLT1* transcript levels is a major cause for RAM size reduction in *JANUS*-RNAi.

PLT1 was reported to positively regulate the expression of *WOX5* (Shimotohno et al., 2018), whose activity defines the QC (Sarkar et al., 2007). We hypothesized that a significant reduction in *PLT1* abundance in *JANUS*-RNAi lines would result in reduced *WOX5* expression. To test this hypothesis, we introduced the *WOX5-pro*:GFP reporter (Blilou et al., 2005) into *JANUS*-RNAi lines as well as in the *imb4-1* and *nrpb10* mutants, both of which were compromised in *PLT1* expression. By examining GFP intensity at the QC of *WOX5pro*:GFP in the wild type (Figure 5A), two *WOX5pro*:GFP lines in *JANUS*-RNAi (Figures 5B and 5C), *WOX5pro*:GFP in *imb4-1* (Figure 5D), and *WOX5pro*:GFP in *nrpb10* (Figure 5E), we determined that *WOX5* transcriptional activity was significantly reduced in the *JANUS*-RNAi, *imb4-1*, and *nrpb10* backgrounds (Figure 5F). RT-qPCR analysis of seedlings from the various genetic materials confirmed a reduction of *WOX5* transcript abundance in the *JANUS*-RNAi, *imb4-1*, and *nrpb10* backgrounds (Figure 5G). These results further support the JANUS-dependent transcription of *PLT1*.

JANUS Is Required for Autotranscriptional Regulation of *PLT1* by Interacting with PLT1

Because JANUS contains no discernible DNA binding domains (Xiong et al., 2019a; Xiong and Li, 2020), we wondered how JANUS might influence *PLT1* transcription in the root meristem, as suggested here, as well as *WOX2* and *PIN7* transcription during embryogenesis (Xiong et al., 2019a). To solve this issue, we performed a Y2H screen using JANUS as the bait. Surprisingly, we identified PLT1 among potential JANUS interactors and confirmed this result by targeted Y2H (Figure 6C) and BiFC (Figure 6B) assays. Upon close examination, we determined that PLT1 interacts with the C terminus of JANUS (Figure 6C) while Pol II components interact with the N-terminal domain of JANUS (Xiong et al., 2019a).

PLT2 was reported to regulate its own transcription (Durgaprasad et al., 2019) and PLT1 was hinted to have a similar autotranscriptional regulatory role (Xu et al., 2020). We first tested whether PLT1 was able to regulate its own transcription. We introduced the *PLT1pro*:CFP reporter into a wild-type line already carrying *UBQ10pro*:GFP-PLT1 (PLT1-OE) and in two *PLT* loss-of-function mutants, the *plt1-4* single mutant and the *plt1-4 plt2-2* double mutant (Aida et al., 2004). By examining CFP intensity at the stem cell niche as a proxy for endogenous *PLT1* transcriptional activity, we determined that PLT1-OE enhanced, whereas *PLT* loss of function reduced, *PLT1* transcriptional activity (Supplemental Figures 6A to 6F). We validated these results by RT-qPCR (Supplemental

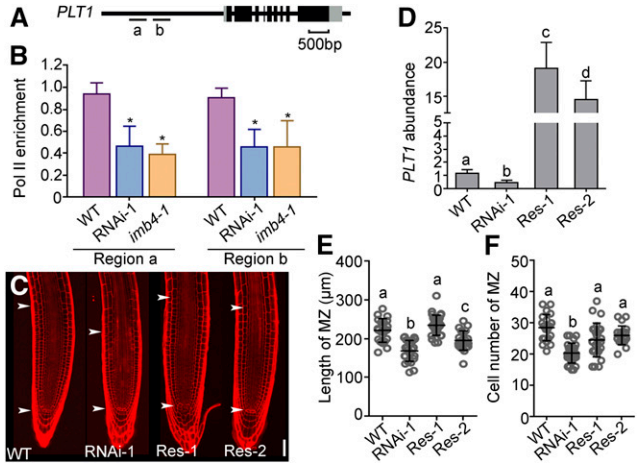

Figure 4. JANUS Mediates Pol II-Dependent *PLT1* Transcription.

(A) Schematic illustration of the *PLT1* genomic locus. Letters (a and b) indicate target regions in ChIP-PCR.

(B) Quantification of ChIP-PCR. Pol II enrichment at *PLT1* is presented as the ratio of *PLT1* (Pol II/input) to *ACTIN* (Pol II/input). Results are means ± SE ($n = 3$). Asterisks indicate significant differences from the wild type (*t* test, $P < 0.05$).

(C) Representative PI-stained roots from the wild type, *35Spro*:*JANUS*-RNAi-1, and two *35Spro*:*JANUS*-RNAi *UBQ10pro*:GFP-PLT1 lines (Res-1 and Res-2). The region of the RAM is indicated by two arrowheads. Bar = 50 μm.

(D) Relative transcript abundance of *PLT1* in the wild type, *35Spro*:*JANUS*-RNAi-1, and two lines of *35Spro*:*JANUS*-RNAi-1 *UBQ10pro*:GFP-PLT1 (Res-1 and Res-2). Values are means ± SE ($n = 3$). RNAs were extracted from seedlings at 5 DAG.

(E) and **(F)** Length **(E)** and cell number **(F)** of the root meristem zone (MZ). Values are means ± SD ($n > 17$).

Different letters in **(D)** to **(F)** indicate significantly different groups (one-way ANOVA, Tukey's multiple comparisons test, $P < 0.05$).

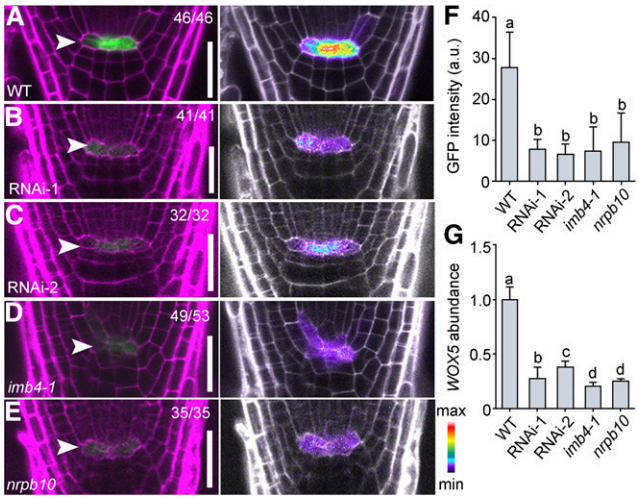

Figure 5. *WOX5* Expression Depends on IMB4, JANUS, and Pol II.

(A) to **(E)** Representative CLSM images of the QC from PI-stained 5-DAG seedling roots expressing the *WOX5pro*:GFP reporter in the Col-0 wild type, two *35Spro*:*JANUS*-RNAi lines (RNAi-1 and RNAi-2), *imb4-1*, and *nrpb10*. Arrowheads point to QC cells. Left, the merge of the RFP (PI; magenta) and GFP channels; right, the GFP channel displayed in pseudocolors, with intensity scale at right bottom. Bars = 50 μm.

(F) and **(G)** GFP intensity **(F)** and *WOX5* abundance **(G)** from the *WOX5pro*:GFP reporter in the Col-0 wild type, two *35Spro*:*JANUS*-RNAi lines (RNAi-1 and RNAi-2), *imb4-1*, and *nrpb10* in the QC cells. a.u. indicates arbitrary units. Values are means ± SD ($n > 30$) in **(F)** and means ± SE ($n = 3$) in **(G)**. RNAs were extracted from seedlings at 5 DAG. Different letters indicate significantly different groups (one-way ANOVA, Tukey's multiple comparisons test, $P < 0.05$).

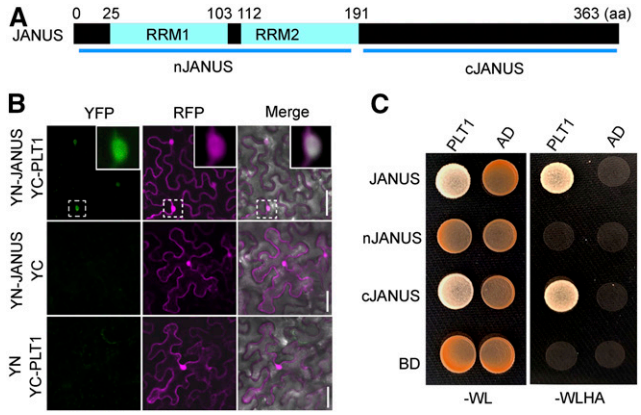

Figure 6. JANUS Interacts with PLT1.

(A) Schematic illustration of JANUS domain organization. RRM indicates RNA-recognition motif; nJANUS indicates the N-terminal domain of JANUS including both RRMs; cJANUS indicates the C-terminal domain of JANUS. aa, amino acids.

(B) A representative BiFC assay showing that JANUS interacts with PLT1 in the nucleus. From left to right: the YFP channel, the RFP channel for RFP expressed from *35Spro*:RFP (magenta), and merges of the YFP, RFP, and transmission channels. Insets are closeups of the dotted squares in the top panels. Bars = 50 μm.

(C) A representative Y2H assay showing that the C terminus of JANUS interacts with PLT1. Yeast colonies transformed with both BD and AD vectors were grown on synthetic minimal medium lacking Trp and Leu (–WL). Positive interactions were determined by growth on synthetic minimal medium lacking Trp, Leu, His, and Ade (–WLHA). Results are representative of three biological replicates.

Figure 6G). Indeed, PLT1 bound to its own promoter sequences based on yeast one-hybrid (Y1H; Figures 7A, 7B, and 7D), ChIP (Figure 7C), and in vitro transcriptional (Figures 7E and 7F) assays. Thus, we conclude that PLT1 positively regulates its own transcription.

Because JANUS interacted with PLT1 and Pol II through nonoverlapping domains, we suspected that JANUS might be critical for the autotranscriptional regulation of PLT1 by recruiting Pol II. To test whether JANUS was required for the autotranscriptional regulation of PLT1, we examined CFP fluorescence from the *PLT1pro*:CFP reporter introduced in the wild type as well as in PLT1-OE, *JANUS*-RNAi, and PLT-OE *JANUS*-RNAi plants. Indeed, the enhanced transcription of endogenous *PLT1* by ectopic *PLT1* was significantly reduced by the downregulation of *JANUS*, based on CFP intensity (Figures 7H and 7I) and RT-qPCR (Figure 7G). Notably, overexpression of *PLT1* did activate the expression of endogenous *PLT1* in *JANUS*-RNAi plants, albeit to a lesser extent than in the wild type (Figures 7H and 7I). If the autoregulation of PLT1 depended solely on JANUS, the overexpression of *PLT1* would be expected to have no or very limited effects on the expression of endogenous *PLT1* in the absence of JANUS. However, there is still residual JANUS present in the *JANUS*-RNAi plants, which may contribute to this upregulation. Alternatively, the autoregulation of PLT1 may not be solely dependent on JANUS. Regardless, we also observed JANUS-dependent PLT1 autoactivation during the formation of the embryonic root pole (Supplemental Figure 7), supporting the idea that JANUS interacts with PLT1 to participate in the autotranscriptional regulation of *PLT1*.

GIF1 Competitively Binds JANUS Away from Pol II to Regulate *PLT1* Transcription

It was unexpected that although both GIF1 and JANUS are regulated by IMB4 for their nuclear accumulation, they play antagonistic roles in root meristem development. In fact, GIF1 appeared in the Arabidopsis Protein Interactome Database as another JANUS interactor (Li et al., 2011). First, we validated the interaction between GIF1 and JANUS by Y2H (Figure 8A) and by BiFC (Supplemental Figure 8) assays. Notably, GIF1 interacted with the N-terminal RRM2 of JANUS (Figure 8A), the same domain responsible for its interaction with Pol II (Xiong et al., 2019a). We thus considered the possibility that GIF1 may interact with the RRM2 domain of JANUS to competitively prevent the JANUS-Pol II interaction, which would explain the antagonistic roles of GIF1 and JANUS during root meristem development. To test this hypothesis, we performed in vitro pull-down (Figure 8B), yeast three-hybrid (Y3H; Figure 8C), and BiFC (Figures 8D and 8E) assays. By all experimental approaches, we determined that GIF1 inhibits the interaction between JANUS and Pol II (Figures 8B to 8E).

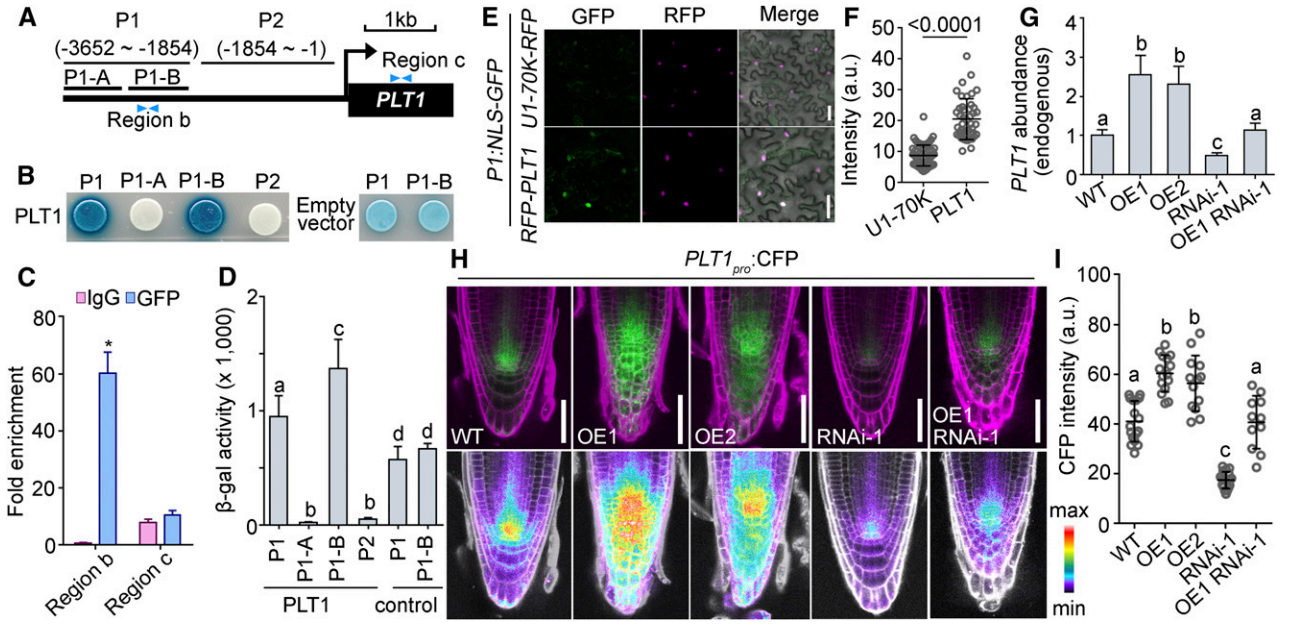

Figure 7. Autotranscriptional Regulation of *PLT1* in RAM Requires JANUS.

(A) Schematic illustration of the promoter and 5′ untranslated region of *PLT1*. P1-A spans from –3652 to –2809 bp; P1-B spans from –2809 to –1854 bp; region b spans from –2047 to –1919 bp; region c spans from 726 to 1103 bp.

(B) Representative Y1H assay. Empty vector used as the negative control shows background activation to the P1 and P1-B regions.

(C) Quantification of ChIP-PCR. Fold enrichment at *PLT1* is presented as the ratio of *PLT1* (ChIP/input) to *ACTIN* (ChIP/input). Results are means ± SE ($n = 3$). Seedlings at 5 DAG were used for the assay. The asterisk indicates a significant difference from the wild type (*t* test, $P < 0.05$).

(D) β-Galactosidase activity from Y1H assays. Control indicates empty vector. Values are means ± SD ($n = 7$). Different letters indicate significantly different groups (one-way ANOVA, Tukey's multiple comparisons test, $P < 0.05$).

(E) and **(F)** Representative CLSM images **(E)** and GFP intensities **(F)** of leaf epidermal cells cotransformed with *P1pro*:NLS-GFP and *35Spro*:RFP-PLT1 (magenta) or *U1pro*-70K-RFP (a nuclear protein as a control; magenta). a.u. indicates arbitrary units. Results are means ± SD ($n > 30$). The P value is shown on top of the bar graph (*t* test). Bars = 50 μm.

(G) to **(I)** Endogenous *PLT1* abundance **(G)**, CLSM images **(H)**, and CFP intensities **(I)** of the *PLT1pro*:CFP reporter in the wild type Col-0, two *UBQ10pro*:GFP-PLT1 lines (OE1 and OE2), *35Spro*:*JANUS*-RNAi (RNAi-1), and *35Spro*:*JANUS*-RNAi *UBQ10pro*:GFP-PLT1 (OE1 RNAi-1). The same *PLT1pro*:CFP transgene was used in all genetic backgrounds. Images in the top row are merges of the CFP and RFP channels (PI; magenta); images in the bottom row are the CFP channel in pseudocolors, for which intensities cover the full range of measured values within each data set (maximum to minimum). Values in **(G)** are means ± SE ($n = 3$). RNAs were extracted from seedlings at 5 DAG. Values in **(I)** are means ± SD ($n > 20$). Fluorescence of the stem cell niche was measured. Different letters indicate significantly different groups (Tukey's multiple comparisons test, $P < 0.05$). Bars = 50 μm.

To provide genetic evidence supporting the antagonistic roles of GIF1 and JANUS in the root meristem, we introduced the *GIF1* loss-of-function mutation *gif1* or the gain-of-function *UBQ10pro*:GFP-GIF1 (Liu et al., 2019) into *JANUS*-RNAi plants and examined root meristem development of the resulting genetic combinations. Downregulating *JANUS* in the *gif1* mutant caused a reduction of the root meristem, as expected based on their opposite phenotypes, rendering it comparable to that of the wild type (Figures 9I and 9J; Supplemental Figure 9). Consistent with the measured root meristem length, *PLT1* abundance returned to wild-type levels in *JANUS*-RNAi *gif1* plants (Figure 9H). By contrast, increasing *GIF1* expression in *JANUS*-RNAi plants caused a further reduction in root meristem length (Figures 9I and 9J; Supplemental Figure 9) and an additional reduction in *PLT1* abundance (Figure 9H). To determine whether the antagonistic roles of GIF1 and JANUS in root meristem development were mediated by *PLT1* transcription, we examined *PLT1* transcriptional activity by examining the activity of the *PLT1pro*:CFP reporter in the wild type (Figure 9A) and in *JANUS*-RNAi (Figure 9B), *gif1* (Figure 9C), *JANUS*-RNAi *gif1* (Figure 9D), GIF1-OE (Figure 9E), and *JANUS*-RNAi GIF1-OE (Figure 9F) plants. A careful examination of the CFP signal (Figure 9G) and RT-qPCR (Figure 9H) confirmed the antagonistic roles of GIF1 and JANUS on *PLT1* transcription. These results demonstrate that JANUS and GIF1 play antagonistic roles in root meristem development, likely through *PLT1* transcription.

In summary, we showed here that JANUS and GIF1 antagonistically regulate *PLT1* transcription (Figure 9K). JANUS positively mediated the autotranscriptional regulation of *PLT1* by binding to both Pol II and PLT1, a role similar to that of subunits of the mediator complex (Dolan and Chapple, 2017). Because JANUS is essential for the autotranscriptional activation of PLT1, JANUS-dependent *PLT1* transcription is critical to amplify differential PLT1 levels established by mitotic dilution and cell-to-cell movement (Mahönen et al., 2014). GIF1, a negative transcriptional regulator of *PLTs* (Ercoli et al., 2018), competitively interacted with JANUS to inhibit its Pol II recruitment. Transcription of *PLT1* was thus spatiotemporally regulated

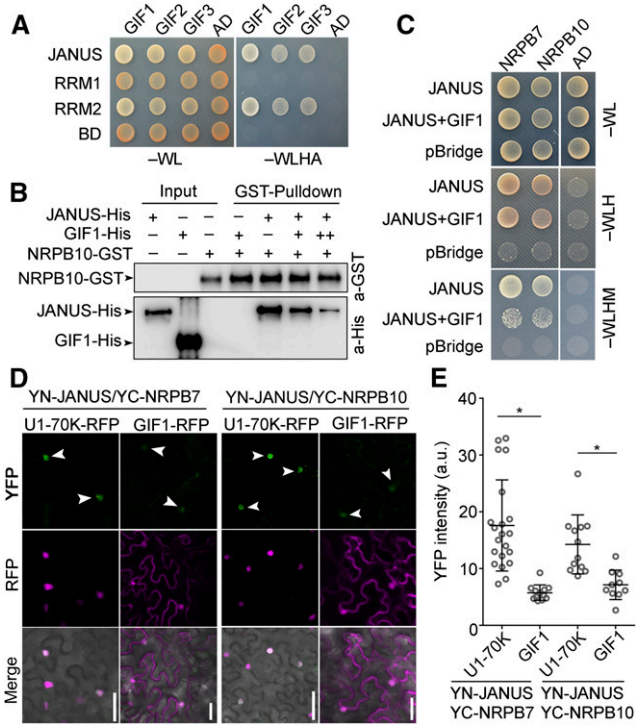

Figure 8. GIF1 Competitively Binds JANUS Away from Pol II.

(A) Y2H assay showing that the RRM2 domain of JANUS interacts with GIFs. Positive interactions were determined by growth on synthetic minimal medium lacking Trp, Leu, His, and Ade (–WLHA). Results are representative of three biological replicates.

(B) In vitro pull-down showing that GIF1 interacts with JANUS to inhibit the interaction between JANUS and the Pol II component NRPB10. Experiments were performed three times with similar results.

(C) Representative Y3H assay showing that GIF1 inhibits the interaction between JANUS and its interacting Pol II components NRPB7 and NRPB10.

(D) and **(E)** Representative CLSM images **(D)** and YFP intensities **(E)** of BiFC assays showing that the positive interaction between YN-JANUS and YC-NRPB7 or YC-NRPB10 is reduced by coexpressing GIF1-RFP but not U1-70K-RFP (magenta), a nuclear marker protein. Arrowheads point at the YFP-positive nuclei. a.u. represents arbitrary units. Values in **(E)** are means ± SD ($n > 11$). Asterisks indicate significant differences (*t* test, $P < 0.05$). Bars in **(D)** = 50 μm.

depending on the GIF1-JANUS interaction and JANUS-dependent autotranscriptional regulation (Figure 9K). The antagonistic *PLT* regulators GIF1 and JANUS both relied on the same importin for their nuclear accumulation (Figure 9K). That two or more cargos in the same pathway are regulated by the same importin may have logistical benefits adopted during evolution.

METHODS

Plant Materials and Growth Conditions

We used Arabidopsis (*Arabidopsis thaliana*) accession Col-0 as the wild type for all experiments. T-DNA insertion mutants in *JANUS* (SALK_008993; *janus*; Xiong et al., 2019a), *NRPB10* (SALK_114301; *nrpb10*; Xiong et al., 2019a), *IMB4* (SALK_049564; *imb4-1*; Liu et al., 2019), *GIF1* (SALK_150407; *gif1*; Lee et al., 2014), and *plt1-4 plt2-2* (Aida et al., 2004) have been described previously. Marker lines carrying *PLT1pro*:CFP (Chen et al., 2011), *PLT2pro*:CFP (Chen et al., 2011), Pro_{WOX5}:GFP (Blilou et al., 2005), *SCRpro*:H2B-YFP (Heidstra et al., 2004), and *CycB1;1pro*:GUS (Chen et al., 2011) have been described. We crossed these marker lines into *janus*/+, *35Spro*:*JANUS*-RNAi, *imb4-1*, *gif1*, *plt1-4*, *plt1-4 plt2-2*, *nrpb10*, *UBQ10-pro*:GFP-GIF1, and *35Spro*:*JANUS*-RNAi *UBQ10pro*:GFP-GIF1. Transgenic plants including *IMB4g*-GFP, *UBQ10pro*:GFP-GIF1, *35Spro*:*JANUS*-RNAi, *JANUSg*-GFP, and *NRPB10g*-GFP were previously described by Liu et al. (2019) and Xiong et al. (2019a). Seedlings and plants were grown in a growth chamber at 20 ± 2°C under long-day conditions (16 h of light/8 h of dark). For growth on plates, we surface-sterilized seeds with 2.6% (v/v) sodium hypochlorite for 10 min, rinsed with sterile water four times, and sowed seeds on half-strength Murashige and Skoog medium. Plates were incubated at 4°C for 2 d and then transferred to a growth chamber at 20 ± 2°C in long-day conditions with 120 to 140 μmol of light (Philips F96T8/TL841/HO/PLUS 86-W bulbs).

DNA Manipulation

We generated all constructs using Gateway technology (Invitrogen) unless otherwise specified. Entry clones were generated in the pENTR/D/TOPO vector (Invitrogen). We used the destination vectors pJG4-5 and pLacZi2u for Y1H (Lin et al., 2007), pDEST-GBKT7 and pDEST-GADT7 (Invitrogen) for Y2H, pET30a and pGEX4T-1 for pull-down assays, pBridge (Clontech) for Y3H, and pSITE::cEYFP-C1 and pSITE::nEYFP-C1 (Martin et al., 2009) for BiFC. Constructs used in Y2H assays, including IMB4-BD, JANUS-AD, JANUS-BD, AtBud13-AD, GIF1-AD, GIF2-AD, GIF3-AD, RRM1-BD, RRM2-BD, NRPB7-AD, NRPB10-AD, and NRPB11-AD, were previously described by Liu et al. (2019) and Xiong et al. (2019a, 2019b). Constructs used in BIFC assays, including YN-JANUS, YN-AtBud13, YC-IMB4, YC-GIF1, YC-GIF2, YC-GIF3, YC-NRPB7, and YC-NRPB10, were were previously described by Liu et al. (2019) and Xiong et al. (2019a, 2019b). For YC-KPNB1 or *PLT1* overexpression, we amplified the full-length coding sequences of *KPNB1* and *PLT1* by PCR with the primer pairs ZY7164/ZY7165 and ZY7197/ZY7198, respectively. The entry vectors were used in LR reactions with the destination vector pSITE::cEYFP-C1 (Martin et al., 2009), *UBQ10pro*:GFP-GW, or *35Spro*:RFP-GW (Wang et al., 2017) to generate YC-KPNB1, *UBQ10pro*:GFP-PLT1, or *35Spro*:RFP-PLT1, respectively.

We performed all PCR amplifications with Phusion hot-start high-fidelity DNA polymerase (Thermo Fisher Scientific) with the annealing temperature and extension times recommended by the manufacturer. All entry vectors were sequenced. All primers are listed in the Supplemental Table.

PCR, RNA Extraction, RT-PCR, and qPCR

We performed genotyping PCR to verify the identity of *janus*, *imb4-1*, *gif1*, and *nrpb10* mutants using the following primers: ZY7860/ZY7861 for *JANUS* and ZY1/ZY7861 for *janus*; ZY4342/ZY4343 for *IMB4* and ZY1/ZY4342 for *imb4-1*; ZY6811/ZY6812 for *GIF1* and ZY1/ZY6812 for *gif1*; and ZY7892/ZY7893 for *NRPB10* and ZY1/ZY7893 for *nrpb10*.

For qPCR analyses, we isolated total RNAs from seedlings 5 DAG using a Qiagen RNeasy plant mini kit according to the manufacturer's instructions with on-column DNase I digestion (Invitrogen). We initiated first-strand cDNA synthesis with oligo(dT) oligonucleotides and SuperScript III reverse transcriptase. We performed RT-qPCR on a Bio-Rad CFX96 real-time system using SYBR Green real-time PCR master mix (Toyobo) as described by Zhou et al. (2013). *GLYCERALDEHYDE-3-PHOSPHATE DEHYDROGENASE* and *ACTIN2* were used as reference genes for qPCR. Primers used are ZY9590/ZY9591 for *PLT1*, ZY9592/ZY9593 for *PLT2*,

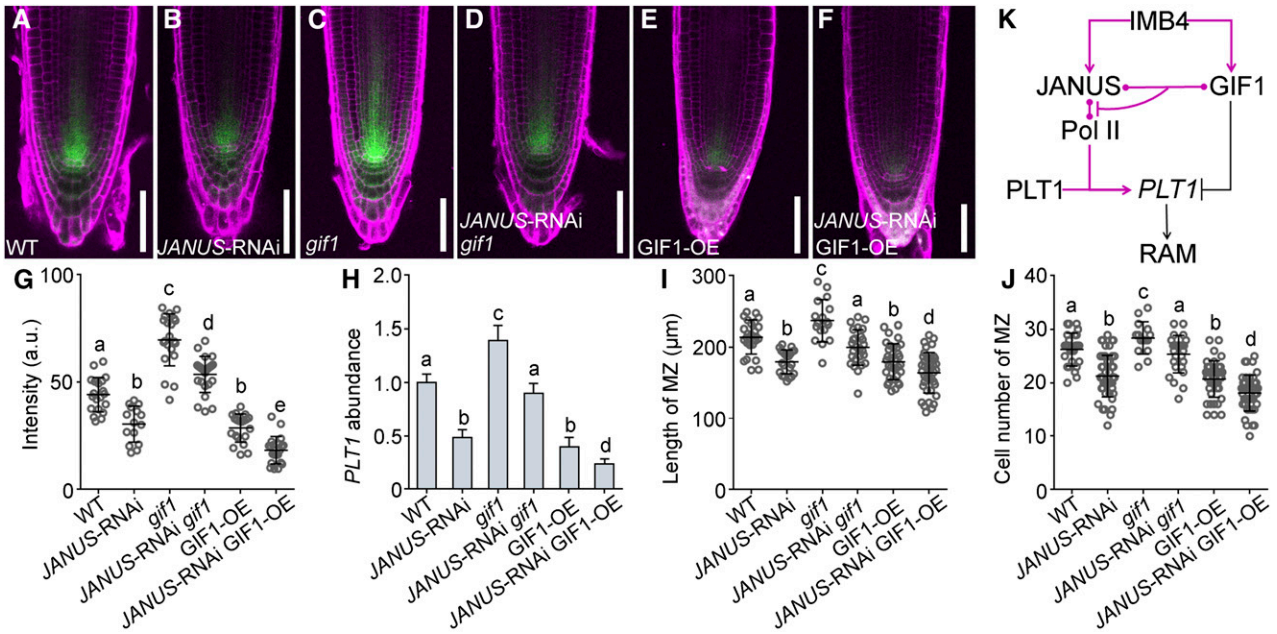

Figure 9. GIF1 and JANUS Antagonistically Mediate the Transcription of *PLT1* and Root Meristem Development.

(A) to **(F)** Representative CLSM images of PI-stained roots expressing the *PLT1pro*:CFP reporter in wild-type Col-0 **(A)**, *35Spro*:*JANUS*-RNAi (RNAi-1; **[B]**), *gif1* **(C)**, *35Spro*:*JANUS*-RNAi *gif1* (*JANUS*-RNAi *gif1*; **[D]**), *UBQ10pro*:GFP-GIF1 (GIF1-OE; **[E]**), and *35Spro*:*JANUS*-RNAi *UBQ10pro*:GFP-GIF1 (*JANUS*-RNAi GIF1-OE; **[F]**). Images are merges of the CFP channel (green) and the RFP channel (magenta). Bars = 50 μm.
(G) CFP intensity at the stem cell niche. a.u. indicates arbitrary units. Values are means ± SD ($n > 20$).
(H) Relative transcript abundance of *PLT1*. Results are means ± SE ($n = 3$). RNAs were extracted from seedlings at 5 DAG.
(I) and **(J)** Length **(I)** and cell number **(J)** of the root meristem zone (MZ). Values are means ± SD ($n > 16$).
Different letters in **(G)** to **(J)** indicate significantly different groups (one-way ANOVA, Tukey's multiple comparisons test, $P < 0.05$).
(K) A working model showing that two cargos regulated by IMB4 perform antagonistic roles in *PLT1* expression and thus root meristem development.

ZY9594/ZY9595 for *SCR*, ZY11346/ZY11347 for the endogenous *PLT1*, WOX5-F/WOX5-R for *WOX5*, and GFP-F/ZY7642 for ectopic *JANUS*. All experiments were repeated in three biological replicates with similar results, and each biological replicate consisted of three technical replicates. All primers are listed in the Supplemental Table.

Y1H Assay

We inserted the P1, P1-A, P1-B, and P2 sequences of the *PLT1* promoter into the pLacZi2u vector after double digestion with *Kpn*I and *Sal*I. We inserted the full-length *PLT1* coding sequence into the pJG4-5 vector (Lin et al., 2007) after double digestion with *Xho*I and *Eco*RI. We cotransformed the two plasmids into the yeast (*Saccharomyces cerevisiae*) strain EGY48. We plated cells onto selective medium (without Ura and Trp) to select transformants. We then grew positive colonies on selective medium without Ura and Trp, supplemented with 20% galactose, 20% raffinose, 50 mL of buffer salts (1.95 g of Na_2HPO_4 and 1.855 g of $NaH_2PO_4 \cdot 2H_2O$), and X-Gal (5-Bromo-4-chloro-3-indolyl β-D-galactoside).

Y2H, Y3H, and BiFC Assays

We performed Y2H assays as described by Xiong et al. (2019a). We cloned the full-length coding sequence for *NRPB7* and *NRPB10* into the pGADT7 vector. For pBridge-JANUS-GIF1, we cloned the coding sequence of *JANUS* into the MCS I site of the pBridge vector (Clontech) fused to the GAL4 DNA binding domain, and the coding sequence of *GIF1* was cloned into the MCS II site of the pBridge vector to generate the "bridge" protein in the absence of Met. Y3H assays were based on the MATCHMAKER GAL4 Two-Hybrid System (Clontech). We cotransformed constructs into yeast strain Y2HGold (Clontech). The presence of the transgenes was confirmed by growth onto synthetic solid medium lacking Trp and Leu. We spotted positive yeast colonies onto plates containing synthetic solid medium lacking Trp, Leu, and His to assess the JANUS-Pol II interaction without the expression of *GIF1*. We used plates containing synthetic solid medium lacking Trp, Leu, His, and Met to induce *GIF1* expression. Interactions were observed after 3 d of incubation at 30°C. BiFC assays were performed as described by Xiong et al. (2019a).

Protein Purification and in Vitro Pull-Downs

For the purification of recombinant proteins in in vitro pull-down assays, we introduced pET30a-JANUS, GST-GIF1, and GST-NRPB10 vectors into BL21 competent cells (DE3). We grew BL21 cells at 37°C in Luria-Bertani medium in the presence of antibiotics (100 μg/mL kanamycin) to an OD_{600} of 0.6 to 0.8. We induced protein accumulation by adding IPTG to a final concentration of 0.5 mM. Cells were further incubated in a shaker set to 90 rpm overnight at 16°C before pellet collection by centrifugation at 12,000 rpm for 10 min at 4°C. We resuspended cell pellets in lysis buffer (20 mM Tris-HCl, pH 7.5, 300 mM NaCl, and 2 mM PMSF) and lysed cells by sonication on ice with seven pulses of 15-s on/off at 30 mW amplitude. We collected the supernatant by centrifugation at 16,000*g* for 30 min at 4°C to completely remove cell debris. We purified the 6× His-JANUS, GST-GIF1, or GST-NRPB10 recombinant protein with Ni-NTA column or glutathione agarose beads (Zhang et al., 2017).

We performed in vitro pull-down assays as described by Wang et al. (2016). We incubated ~1 μg each of GST or GST-NRPB10 protein to 25 μL of glutathione-Sepharose beads for 1 h at 4°C. We then incubated bound beads with 1 μg of 6× His-JANUS protein for another 1 h at 4°C. After three washes with 1× PBS buffer, we eluted the beads with 40 μL of 10 mM glutathione in 50 mM Tris (pH 8.0), mixed with a loading buffer, and then boiled at 100°C for 10 min. We loaded ~15 μL of each boiled sample for SDS-PAGE and immunoblot analysis with an anti-His antibody (Beyotime; 1:1000 dilution) and an anti-GST antibody (Beyotime; 1:1000 dilution). For secondary antibodies, we used a goat anti-mouse IgG horseradish peroxidase (Beyotime; 1:1000 dilution) and a goat anti-rabbit IgG horseradish peroxidase (Beyotime; 1:1000 dilution).

For pull-down assays to test whether a high concentration of GIF1 affects the JANUS-NRPB10 interaction, we added 1 μg of purified GST-NRPB10 and 6× His-JANUS to each sample. We added purified GST-GIF1 according to the concentration gradient. We then used the glutathione-Sepharose beads to pull down proteins. The sequential procedures and buffers were the same as those described above.

Fluorescence Imaging and Quantification

We captured all fluorescence images on a Zeiss LSM880 laser scanning microscope with a 20 or 40/1.3 oil objective. Fluorescence of GFP, YFP, mCherry, and PI staining was captured using the following excitation/emission settings: 488 nm/505 to 550 nm for GFP, 458 nm/463 to 500 nm for CFP, 514 nm/530 to 590 nm for YFP, and 561 nm/600 to 650 nm for mCherry and PI staining. Image processing was performed with the LSM image-processing software (Zeiss). We imaged embryos or roots of 5-DAG seedlings from the *SCRpro*:H2B-YFP, *PLT1pro*:CFP, *PLT2pro*:CFP, or *JANUSg*-GFP plants by CLSM. We defined regions of interest (ROIs) as the nuclei for *SCRpro*:H2B-YFP and *JANUSg*-GFP in embryogenesis or upon ivermectin treatment or in BiFC assays as in Figure 8. We defined ROIs as the entire stem cell niche for *PLT1pro*:CFP and *PLT2pro*:CFP. The ROI was defined as the entire embryonic root pole for *PLT1pro*:CFP during late embryogenesis. We quantified fluorescence intensity using 40 to 60 cells from 15 to 20 roots for each genetic background or each treatment with ImageJ. We determined statistical significance by Student's *t* test or one-way ANOVA (Tukey's multiple comparisons test).

Cell Fractionation and Immunoblot Analysis

We performed cell fractionation as described by Wierzbicki et al. (2008) with slight modifications. Specifically, we ground 2 g of seedlings into powder in liquid nitrogen, suspended the resulting powder in 20 mL of Honda buffer (20 mM HEPES-KOH, pH 7.4, 0.44 M Suc, 1.25% [v/v] Ficoll, 2.5% [w/v] Dextran T40, 10 mM $MgCl_2$, 0.5% [v/v] Triton X-100, 5 mM DTT, 1 mM PMSF, and 1% [w/v] plant protease inhibitors) before filtering through two layers of Miracloth and centrifugation at 5000*g* for 20 min. We collected the supernatant as the cytosolic fraction. We washed the pellets five times, each time with 1 mL of Honda buffer. We obtained total nuclear proteins by adding 3 volumes of 1% (w/v) SDS directly to the nucleus pellet, followed by boiling at 95°C for 10 min. We mixed equal volumes of each fraction with loading buffer, boiled, gel-separated, and subjected them to immunoblot analysis. Immunolabeling of GFP-JANUS was performed using an anti-GFP antibody (Beyotime; 1:1000 dilution). Anti-histone H3 (Beyotime; 1:1000 dilution) and anti-cFBPase (Agrisera; 1:5000 dilution) were used as the nuclear and cytoplasmic markers, respectively. Quantification of total proteins was performed using Gel Image System 4.1.2 (Bio-Tanon).

ChIP

We performed ChIP assays as described by Saleh et al. (2008). We harvested 2 g of wild-type, *imb4-1*, and *35Spro*:*JANUS*-RNAi seedlings at 12 DAG in cross-linking buffer (0.4 M sucrose, 10 mM Tris-HCl, pH 8.0, 1 mM PMSF, 1 mM EDTA, and 1% formaldehyde) for 10 min under vacuum infiltration and then halted in 2 M Gly. After the addition of 5 μg of anti-Pol II antibodies (Abcam) to the chromatin and incubation at 4°C overnight, we added agarose beads conjugated with protein A and protein G and incubated at 4°C for 2.5 h. After reverse cross-linking, we eluted DNA and dissolved it in 20 μL of water. We diluted the immunoprecipitated DNA with sterile water before quantification by real-time PCR. Real-time PCR data were normalized to *ACTIN*. We express the enrichment of Pol II at the *PLT1* genomic locus as the ratio of (Pol II *PLT1*/input *PLT1*) to (Pol II *ACTIN*/input *ACTIN*). For PLT1 autoactivation, we performed ChIP assays using anti-GFP antibodies on 5-d-old wild-type or *35Spro*:GFP-PLT1 seedlings. The enrichment of PLT1 at its genomic locus is given as the ratio of (ChIP *PLT1*/input *PLT1*) to (ChIP *ACTIN*/input *ACTIN*). Primers used are ZY9923/ZY9924 for *PLT1* fragment a, ZY9925/ZY9926 for *PLT1* fragment b, and ZY9590/ZY9591 for *PLT1* fragment c. Primers are listed in the Supplemental Table.

Ivermectin Treatment

We incubated *JANUSg*-GFP seedlings at 5 DAG in liquid half-strength Murashige and Skoog medium supplemented with DMSO or 5 to 15 μM ivermectin (Sigma-Aldrich PHR1380-1G; predissolved in DMSO) for 8 h before imaging.

Accession Numbers

Sequence data in this article can be found in The Arabidopsis Information Resource under the following accession numbers: At2g18510 (*JANUS*), At5g28640 (*GIF1*), At1g01160 (*GIF2*), At4g00850 (*GIF3*), At4g27640 (*IMB4*), At5g59180 (*NRPB7*), At1g11475 (*NRPB10*), At3g20840 (*PLT1*), At1g51190 (*PLT2*), At3g54220 (*SCR*), At3g11260 (*WOX5*), At1g31870 (*AtBud13*), and At5g53480 (*KPNB1*).

Supplemental Data

Supplemental Figure 1. IMB4 mediates nuclear accumulation of GIF1 in RAM.

Supplemental Figure 2. Nuclear accumulation of JANUS in early embryogenesis is independent of *IMB4*.

Supplemental Figure 3. Ivermectin inhibits the nuclear accumulation of JANUS.

Supplemental Figure 4. JANUS positively regulates embryonic root meristem activity.

Supplemental Figure 5. Pol II positively regulates root meristem activity and *PLT1* transcription.

Supplemental Figure 6. Self-transcriptional regulation of *PLT1*.

Supplemental Figure 7. Auto-transcriptional regulation of *PLT1* in late embryogenesis requires JANUS.

Supplemental Figure 8. GIFs interact with JANUS.

Supplemental Figure 9. GIF1 and JANUS antagonistically mediate RAM.

Supplemental Table. Oligos used in this study.

ACKNOWLEDGMENTS

We thank the ABRC for mutant seeds, Ben Scheres for *SCRpro*:H2B-YFP, Qian Chen for the *PLT1pro*:CFP and *PLT2pro*:CFP marker lines, Xu-Gang

Li for the *plt1-4* and *plt1-4 plt2-2* mutants, and Xian Sheng Zhang for the *CycB1;1pro*:GUS and *WOX5pro*:GFP lines. This work was supported by the National Natural Science Foundation of China (grants 31771558 and 31970332 to S.L.).

AUTHOR CONTRIBUTIONS

F.X. conceptualized the study. F.X., S.L., and Y.Z. created the methodology. F.X., B.-K.Z., H.-H.L., G.W., J.-H.W., and Y.-N.W. performed the research. F.X. wrote the original draft of the article, and S.L. and Y.Z. were responsible for the editing and review. S.L. and Y.Z. supervised the study. Funding was acquired by S.L.

Received February 11, 2020; revised August 31, 2020; accepted September 21, 2020; published September 28, 2020.

REFERENCES

Aida, M., Beis, D., Heidstra, R., Willemsen, V., Blilou, I., Galinha, C., Nussaume, L., Noh, Y.S., Amasino, R., and Scheres, B. (2004). The *PLETHORA* genes mediate patterning of the *Arabidopsis* root stem cell niche. Cell **119:** 109–120.

Blilou, I., Xu, J., Wildwater, M., Willemsen, V., Paponov, I., Friml, J., Heidstra, R., Aida, M., Palme, K., and Scheres, B. (2005). The PIN auxin efflux facilitator network controls growth and patterning in *Arabidopsis* roots. Nature **433:** 39–44.

Chen, Q., et al. (2011). The basic helix-loop-helix transcription factor MYC2 directly represses *PLETHORA* expression during jasmonate-mediated modulation of the root stem cell niche in Arabidopsis. Plant Cell **23:** 3335–3352.

Cruz-Ramírez, A., Díaz-Triviño, S., Wachsman, G., Du, Y., Arteága-Vázquez, M., Zhang, H., Benjamins, R., Blilou, I., Neef, A.B., Chandler, V., and Scheres, B. (2013). A SCARECROW-RETINOBLASTOMA protein network controls protective quiescence in the *Arabidopsis* root stem cell organizer. PLoS Biol. **11:** e1001724.

Dolan, L., Janmaat, K., Willemsen, V., Linstead, P., Poethig, S., Roberts, K., and Scheres, B. (1993). Cellular organisation of the *Arabidopsis thaliana* root. Development **119:** 71–84.

Dolan, W.L., and Chapple, C. (2017). Conservation and divergence of mediator structure and function: Insights from plants. Plant Cell Physiol. **58:** 4–21.

Durgaprasad, K., Roy, M.V., Venugopal M, A., Kareem, A., Raj, K., Willemsen, V., Mähönen, A.P., Scheres, B., and Prasad, K. (2019). Gradient expression of transcription factor imposes a boundary on organ regeneration potential in plants. Cell Rep. **29:** 453–463.e3.

Ercoli, M.F., Ferela, A., Debernardi, J.M., Perrone, A.P., Rodriguez, R.E., and Palatnik, J.F. (2018). GIF transcriptional coregulators control root meristem homeostasis. Plant Cell **30:** 347–359.

Galinha, C., Hofhuis, H., Luijten, M., Willemsen, V., Blilou, I., Heidstra, R., and Scheres, B. (2007). PLETHORA proteins as dose-dependent master regulators of Arabidopsis root development. Nature **449:** 1053–1057.

Heidstra, R., and Sabatini, S. (2014). Plant and animal stem cells: Similar yet different. Nat. Rev. Mol. Cell Biol. **15:** 301–312.

Heidstra, R., Welch, D., and Scheres, B. (2004). Mosaic analyses using marked activation and deletion clones dissect *Arabidopsis* SCARECROW action in asymmetric cell division. Genes Dev. **18:** 1964–1969.

Heyman, J., Kumpf, R.P., and De Veylder, L. (2014). A quiescent path to plant longevity. Trends Cell Biol. **24:** 443–448.

Laux, T. (2003). The stem cell concept in plants: A matter of debate. Cell **113:** 281–283.

Lee, B.H., Wynn, A.N., Franks, R.G., Hwang, Y.S., Lim, J., and Kim, J.H. (2014). The *Arabidopsis thaliana* GRF-INTERACTING FACTOR gene family plays an essential role in control of male and female reproductive development. Dev. Biol. **386:** 12–24.

Li, P., Zang, W., Li, Y., Xu, F., Wang, J., and Shi, T. (2011). AtPID: The overall hierarchical functional protein interaction network interface and analytic platform for *Arabidopsis*. Nucleic Acids Res. **39:** D1130–D1133.

Lin, R., Ding, L., Casola, C., Ripoll, D.R., Feschotte, C., and Wang, H. (2007). Transposase-derived transcription factors regulate light signaling in *Arabidopsis*. Science **318:** 1302–1305.

Liu, H.H., Xiong, F., Duan, C.Y., Wu, Y.N., Zhang, Y., and Li, S. (2019). Importin β4 mediates nuclear import of GRF-interacting factors to control ovule development in Arabidopsis. Plant Physiol. **179:** 1080–1092.

Luo, Y., Wang, Z., Ji, H., Fang, H., Wang, S., Tian, L., and Li, X. (2013). An *Arabidopsis* homolog of importin β1 is required for ABA response and drought tolerance. Plant J. **75:** 377–389.

Mähönen, A.P., Ten Tusscher, K., Siligato, R., Smetana, O., Díaz-Triviño, S., Salojärvi, J., Wachsman, G., Prasad, K., Heidstra, R., and Scheres, B. (2014). PLETHORA gradient formation mechanism separates auxin responses. Nature **515:** 125–129.

Martin, K., Kopperud, K., Chakrabarty, R., Banerjee, R., Brooks, R., and Goodin, M.M. (2009). Transient expression in *Nicotiana benthamiana* fluorescent marker lines provides enhanced definition of protein localization, movement and interactions in planta. Plant J. **59:** 150–162.

Petricka, J.J., Winter, C.M., and Benfey, P.N. (2012). Control of *Arabidopsis* root development. Annu. Rev. Plant Biol. **63:** 563–590.

Rodriguez, R.E., Ercoli, M.F., Debernardi, J.M., Breakfield, N.W., Mecchia, M.A., Sabatini, M., Cools, T., De Veylder, L., Benfey, P.N., and Palatnik, J.F. (2015). MicroRNA miR396 regulates the switch between stem cells and transit-amplifying cells in *Arabidopsis* roots. Plant Cell **27:** 3354–3366.

Sabatini, S., Heidstra, R., Wildwater, M., and Scheres, B. (2003). SCARECROW is involved in positioning the stem cell niche in the *Arabidopsis* root meristem. Genes Dev. **17:** 354–358.

Saleh, A., Alvarez-Venegas, R., and Avramova, Z. (2008). An efficient chromatin immunoprecipitation (ChIP) protocol for studying histone modifications in *Arabidopsis* plants. Nat. Protoc. **3:** 1018–1025.

Santuari, L., et al. (2016). The *PLETHORA* gene regulatory network guides growth and cell differentiation in *Arabidopsis* roots. Plant Cell **28:** 2937–2951.

Sarkar, A.K., Luijten, M., Miyashima, M., Lenhard, M., Hashimoto, T., Nakajima, K., Scheres, B., Heidstra, R., and Laux, T. (2007). Conserved factors regulate signalling in Arabidopsis thaliana shoot and root stem cell organizers. Nature **446:** 811–814.

Scheres, B. (2007). Stem-cell niches: Nursery rhymes across kingdoms. Nat. Rev. Mol. Cell Biol. **8:** 345–354.

Sena, G., Wang, X., Liu, H.Y., Hofhuis, H., and Birnbaum, K.D. (2009). Organ regeneration does not require a functional stem cell niche in plants. Nature **457:** 1150–1153.

Shimotohno, A., Heidstra, R., Blilou, I., and Scheres, B. (2018). Root stem cell niche organizer specification by molecular convergence of PLETHORA and SCARECROW transcription factor modules. Genes Dev. **32:** 1085–1100.

van den Berg, C., Willemsen, V., Hage, W., Weisbeek, P., and Scheres, B. (1995). Cell fate in the *Arabidopsis* root meristem determined by directional signalling. Nature **378:** 62–65.

Wang, J.G., Feng, C., Liu, H.H., Feng, Q.N., Li, S., and Zhang, Y. (2017). AP1G mediates vacuolar acidification during synergid-controlled pollen tube reception. Proc. Natl. Acad. Sci. USA **114:** E4877–E4883.

Wang, T., Liang, L., Xue, Y., Jia, P.F., Chen, W., Zhang, M.X., Wang, Y.C., Li, H.J., and Yang, W.C. (2016). A receptor heteromer mediates the male perception of female attractants in plants. Nature **531:** 241–244.

Watt, F.M., and Hogan, B.L. (2000). Out of Eden: Stem cells and their niches. Science **287:** 1427–1430.

Weigel, D., and Jürgens, G. (2002). Stem cells that make stems. Nature **415:** 751–754.

Wierzbicki, A.T., Haag, J.R., and Pikaard, C.S. (2008). Noncoding transcription by RNA polymerase Pol IVb/Pol V mediates transcriptional silencing of overlapping and adjacent genes. Cell **135:** 635–648.

Wysocka-Diller, J.W., Helariutta, Y., Fukaki, H., Malamy, J.E., and Benfey, P.N. (2000). Molecular analysis of SCARECROW function reveals a radial patterning mechanism common to root and shoot. Development **127:** 595–603.

Xiong, F., and Li, S. (2020). SF3b4: A versatile player in eukaryotic cells. Front. Cell Dev. Biol. **8:** 14.

Xiong, F., Liu, H.H., Duan, C.Y., Zhang, B.K., Wei, G., Zhang, Y., and Li, S. (2019a). *Arabidopsis* JANUS regulates embryonic pattern formation through Pol II-mediated transcription of *WOX2* and *PIN7*. iScience **19:** 1179–1188.

Xiong, F., Ren, J.J., Yu, Q., Wang, Y.Y., Kong, L.J., Otegui, M.S., and Wang, X.L. (2019b). AtBUD13 affects pre-mRNA splicing and is essential for embryo development in *Arabidopsis*. Plant J. **98:** 714–726.

Xu, J., Hofhuis, H., Heidstra, R., Sauer, M., Friml, J., and Scheres, B. (2006). A molecular framework for plant regeneration. Science **311:** 385–388.

Xu, M., Gu, X., Liang, N., Bian, X., Wang, H., Qin, Y., Pi, L., and Wu, S. (2020). Intersected functional zone of transcriptional regulators patterns stemness within stem cell niche of root apical meristem. J. Integr. Plant Biol. **62:** 897–911.

Zhang, Z., Tucker, E., Hermann, M., and Laux, T. (2017). A molecular framework for the embryonic initiation of shoot meristem stem cells. Dev. Cell **40:** 264–277.e4.

Zhou, L.Z., Li, S., Feng, Q.N., Zhang, Y.L., Zhao, X., Zeng, Y.L., Wang, H., Jiang, L., and Zhang, Y. (2013). PROTEIN S-ACYL TRANSFERASE10 is critical for development and salt tolerance in *Arabidopsis*. Plant Cell **25:** 1093–1107.